Supplement of The Cryosphere, 19, 283–301, 2025
https://doi.org/10.5194/tc-19-283-2025-supplement

The Cryosphere Open Access EGU

Supplement of

Present-day mass loss rates are a precursor for West Antarctic Ice Sheet collapse

Tim van den Akker et al.

Correspondence to: Tim van den Akker (t.vandenakker@uu.nl)

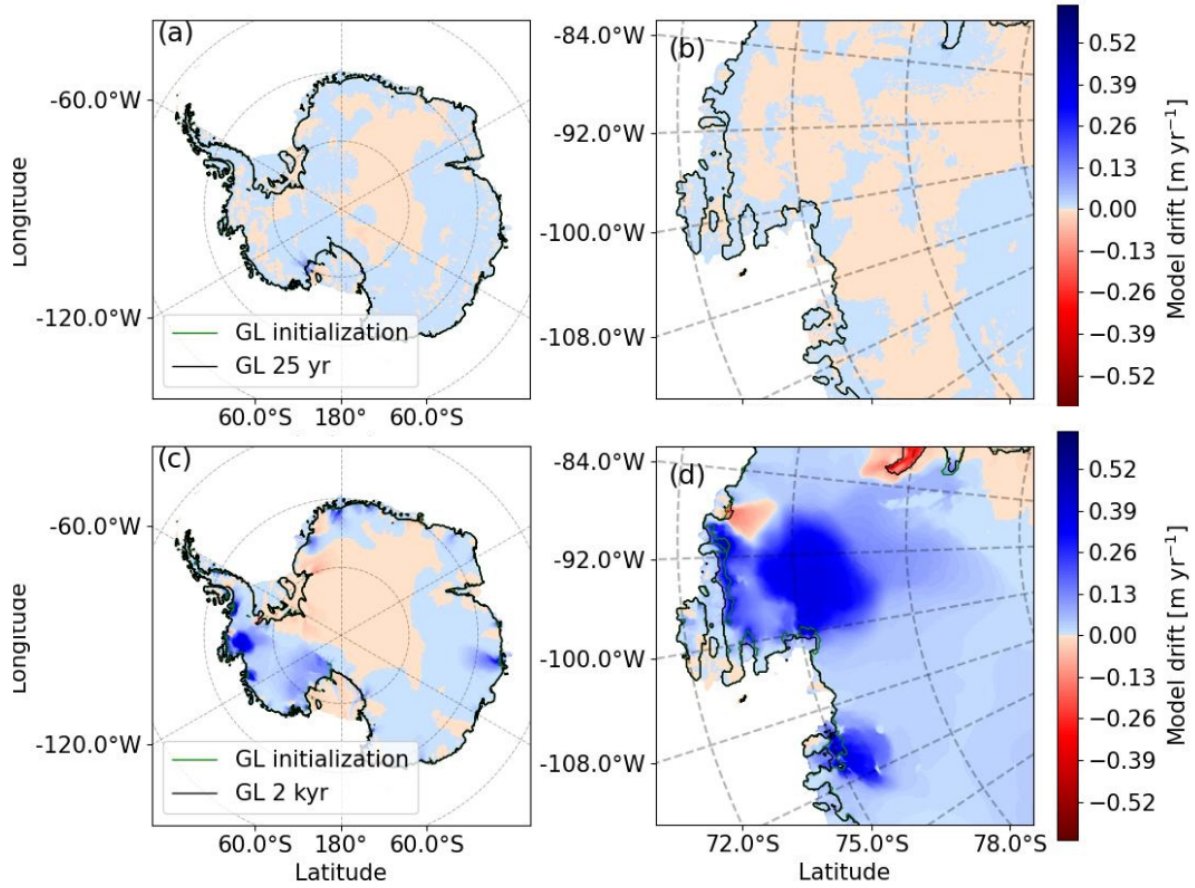

Figure S1. Average model drift in terms of thickness change rates of the transient simulation. (Top) Mean model drift in the first 25 years after initialization for all Antarctica (left) and the ASE region (right). **(Bottom)** Mean model drift during a continuation of 2000 yr. The modelled grounding line is shown at initialization (green) and after 25 yr and 2000 yr for the upper and lower panel, respectively (black).

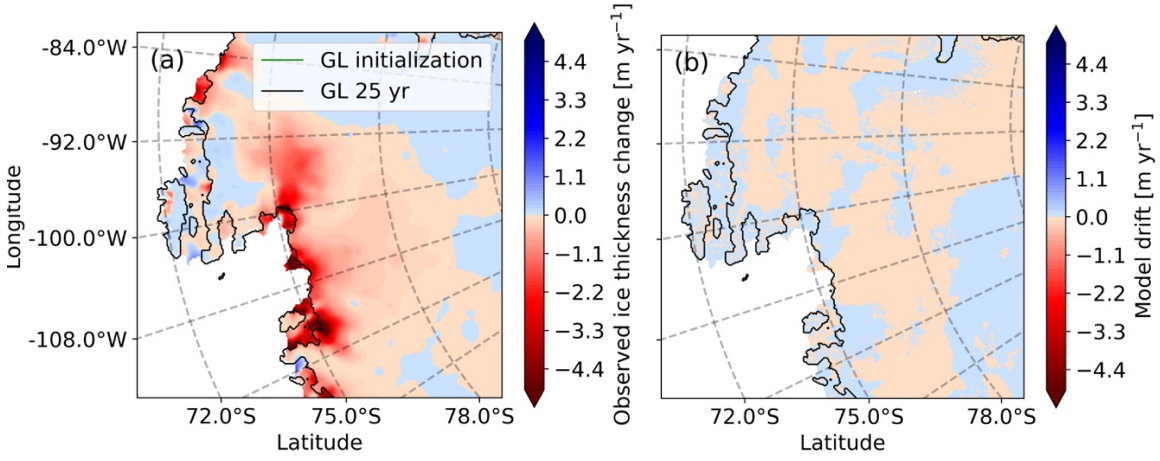

Figure S2. Observed mass change rates (left) and the instantaneous model drift in the default experiment (right) in the ASE region. (left) Mass change rates of (Smith et al., 2020). (right) Mean model drift in the first 25 years after the transient initialization.

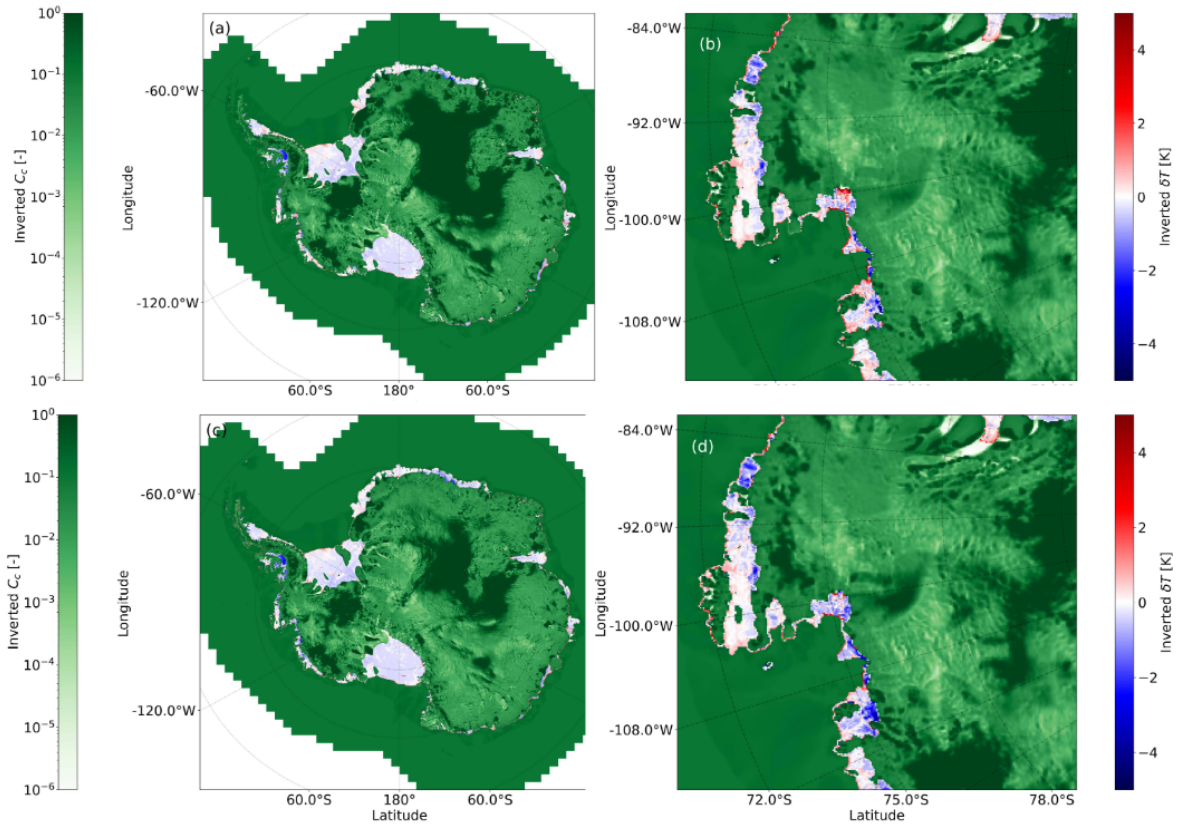

Fig S3. Inverted quantities in two CISM initializations (top, transient initialization. Bottom, equilibrium initialization): C_c in the friction parameterization (Eq 1.1) and δT in the basal melt parametrization (Eq 1.5) in the transient initialization under floating ice shelves for the whole AIS (a) and zoomed in to the ASE (b), and similarly for the equilibrium initialization, (c) and (d).

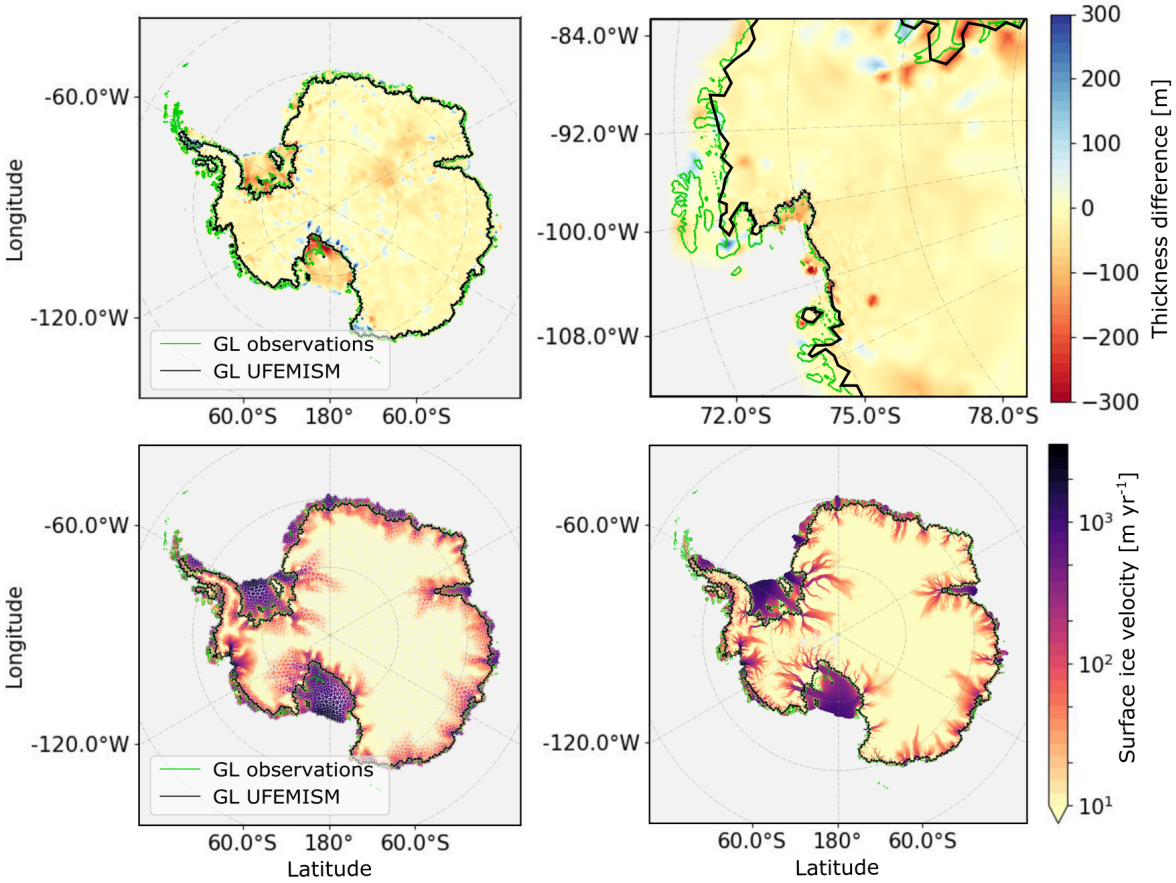

Figure S4 UFEMISM initialzitation. (**Top**) Ice thickness difference between the UFEMISM initial state and observations for (left) the AIS and (right) the Amundsen Sea region. The thickness RMSE is 80.3 m for the full domain and 86.9 m for the Amundsen Basin. (**Bottom**) Antarctic ice surface speed (m/yr, log scale) for (left) the end of the UFEMISM initialization procedure (plotted on the triangular mesh) and (right) observations (Rignot et al., 2019). RMSE is 209 m/yr for the full domain, 148 m/yr for ASE, and 381 m/yr for ASE shelves only.

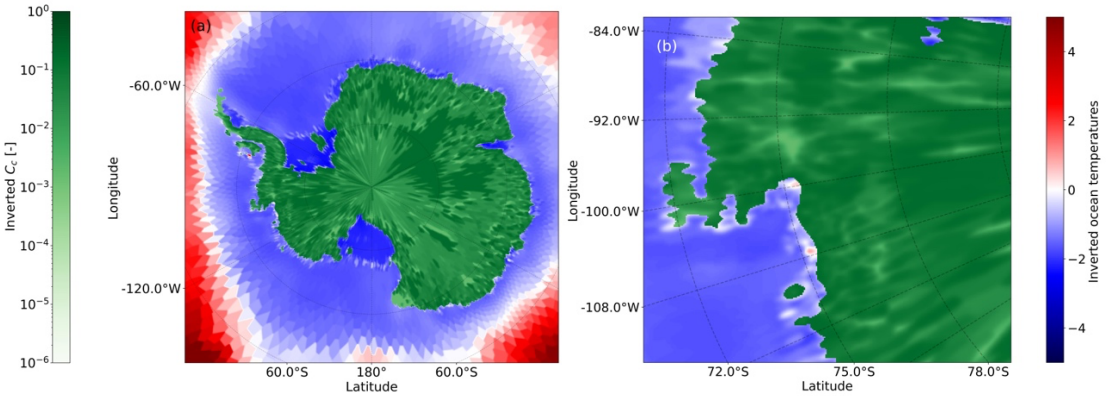

Fig S5. Inverted quantities in the UFEMISM initialization: C_c ($tan\,\phi$ in Eq 1.8) in the friction parameterization and the ocean temperatures (the sum of $TF_{\text{base}} + \delta T$ in Eq 1.5) in the basal melt paramerization in the transient initialization under floating ice shelves for the whole AIS (a) and zoomed in to the ASE (b).

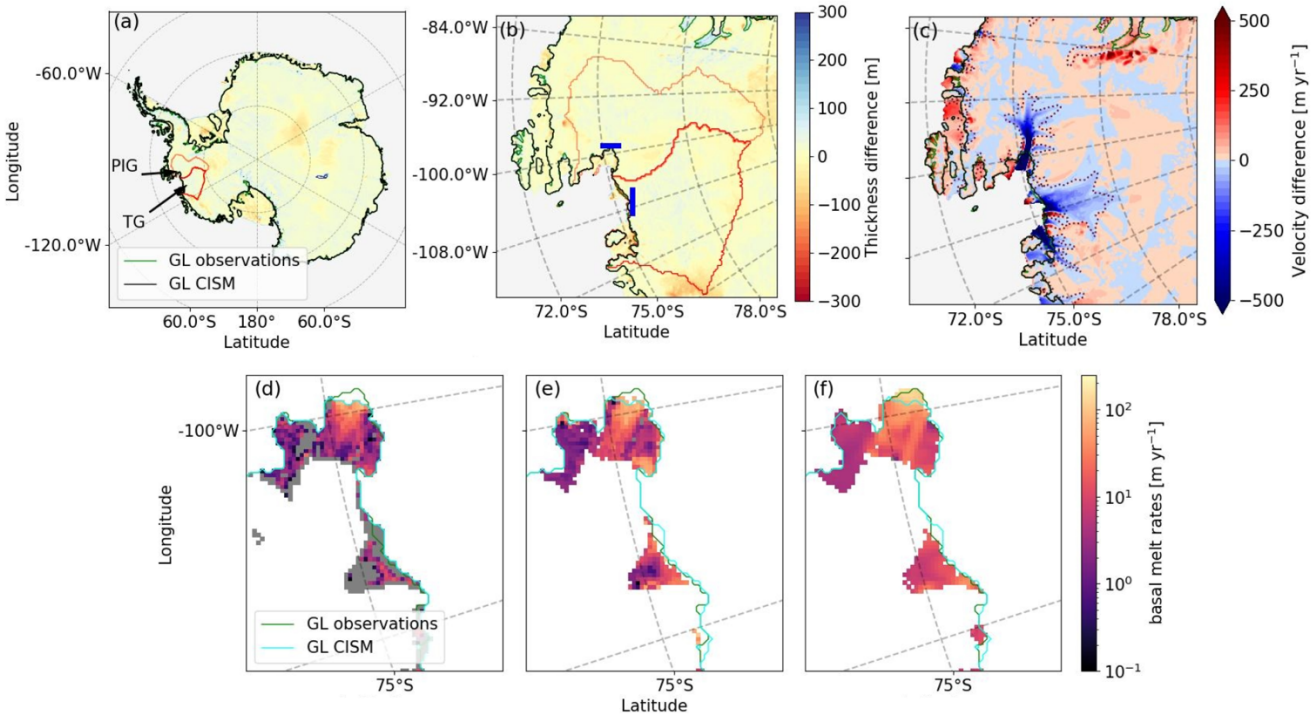

Figure S6. Modeled present-day state for the equilibrium initialisations. (Top) Thickness difference with thickness RMSE = 31 m for the full domain (left) and 24.4 m for the ASE (middle). Black contour lines represent the modelled grounding line. The observed grounding line (green) is only visible where the modelled and observed grounding line deviate in position, for example at the PIG grounding line. Red and orange contours are drawn around the TG and PIG basins, respectively. (right) Surface ice velocity difference with respect to observations (Rignot et al., 2019). Positive differences indicate locations where CISM overestimates velocities. Observed surface velocities of 100 (outer) and 500 (inner) m yr^{-1} are contoured by black dots, to highlight fast-flowing regions with large velocities and gradients. For the ASE, the velocity RMSE = 160 m yr^{-1} (cf. RMS = 178 m yr^{-1}, max = 2025 m yr^{-1}). For ASE shelves only, the velocity RMSE = 420 m yr^{-1} (cf. RMS = 396 m yr^{-1}, max = 2025 m yr^{-1}). **(Bottom)** Basal melt rates (zero basal melt is marked by grey cells, white cells contain no data) of CISM (left, integrated flux of 51 Gt yr^{-1}), ref (Adusumilli et al., 2020) (middle, integrated flux of 94 Gt yr^{-1}) and ref(Rignot et al., 2013) (right, integrated flux of 149 Gt yr^{-1}).

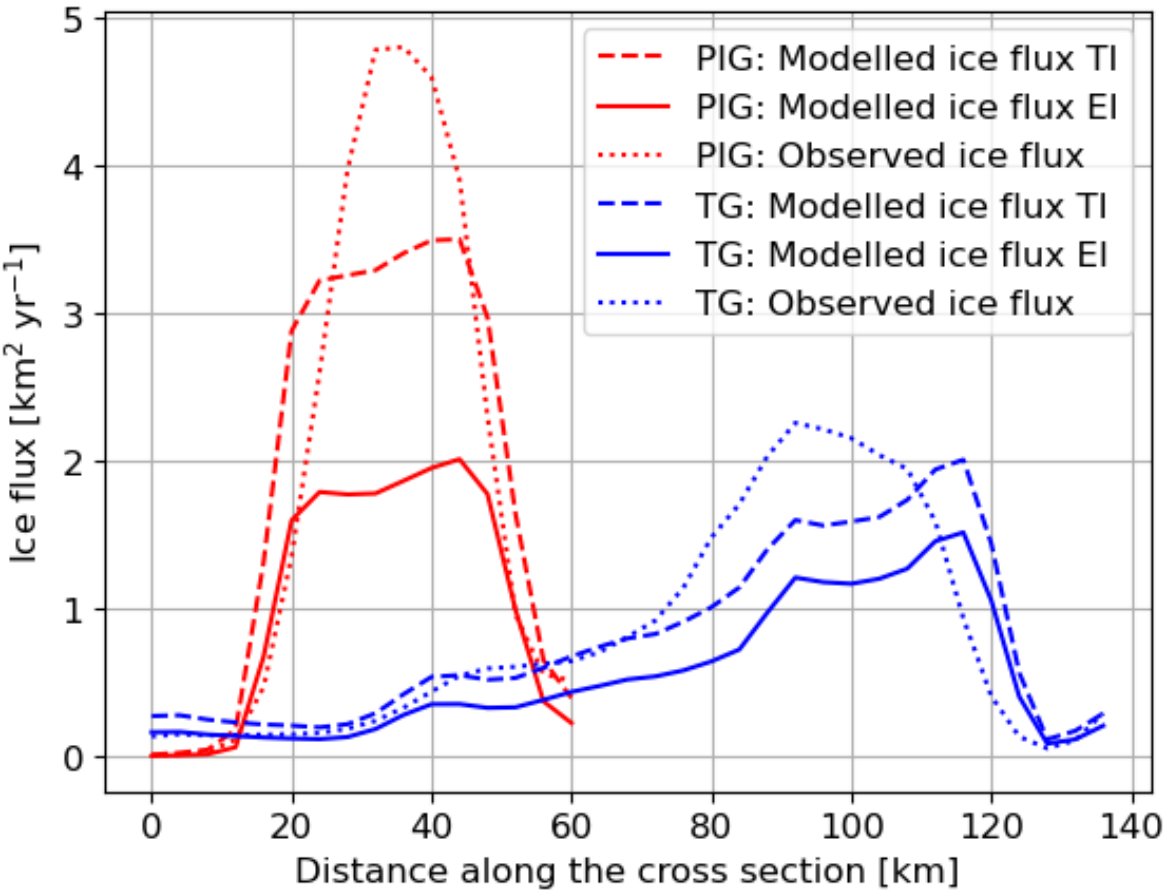

Figure S7. Fluxes across the blue lines shown in Fig. 1. Flux across the cross sections in Fig. 1b for the Transient Initialization (TI) and Equilibrium Initialization (EI), and the observations (Morlighem et al., 2020) for PIG (red) and TG (blue). Distance along the cross section is for PIG from left to right and for TG top to bottom shown in blue stripes in Fig. 1b. The fluxes for the TG cross section are 19.3 (EI), 27.6 (TI) and 28.3 (Obs) km^2 yr^{-1}. The fluxes for the PIG cross section are 17.0 (EI), 30.4 (TI), 31.1 (Obs)) km^2 yr^{-1}.

Table S1. Description of the sensitivity analysis done in Figure 3. The experiments are listed in the same order as in Table 1.

8km grid, partial melt parameterization This run tests the sensitivity to grid resolution in combination with a partial melt parameterization (PMP, see (Leguy et al., 2021) applied at the grounding line. This run has its own initialization.
High basal melt versus thermal forcing γ_0 in Eq. 1.5 modulates the relation between ocean temperature and basal melt rate. A higher value means a higher sensitivity of the basal melt rate to temperature changes. Since ocean thermal forcing increases with depth in the Amundsen Sea, melt rates increase with depth: a higher (lower) value for γ_0 increases (decreases) the sensitivity of melt rates to the ice draft depth, thereby speeding up (slowing down) ice retreat. We use γ_0= 50,000 m yr^{-1}, the largest value reported in (Jourdain et al., 2020). This run is done with the default initialization (with γ_0 = 30,000 m yr^{-1}), but the ocean temperatures are recalculated at $t = 0$, so that the basal melt rates at $t = 0$ are unchanged from the initialization with γ_0 = 30,000 m yr^{-1} .
Larger flow factor (softer ice) Glen's flow law (see Eq. S1, with $\tau_{i,j}$, $A(T^*)$, ϵ_e and $\epsilon_{i,j}$ respectively the deviatoric stress, the temperature dependent rate factor, the effective strain rate and the strain rate) is multiplied by a factor *E*, referred to as the flow enhancement factor. A value higher (lower) than 1 means that the effective viscosity of the ice is smaller (larger) for given strain rates, that the ice is generally softer (stiffer), and the velocities are higher (lower). The default values are 1.0 for grounded ice (no correction) and 0.5 for floating ice. In this sensitivity run, we set *E* = 1.5 for grounded ice and *E* = 1 for floating ice. A new initialized state is obtained. $$\tau_{i,j} = \mathrm{E} * A(T^*)^{\frac{-1}{n}} \epsilon_e^{\frac{1-n}{n}} \epsilon_{i,j} \quad \text{(S1)}$$
No ocean connection For ice resting on bedrock below sea level, we decrease the effective pressure based on the height above floatation to account for a possible connection to the ocean; see Eq. 1.3 and (Leguy et al., 2014; Berdahl et al., 2023). In this simulation we set *p = 0* (instead of the default, *p = 0.5*), implying overburden pressure everywhere. A new initial state is obtained.
Schoof basal sliding law We apply the Schoof basal sliding law described in (Leguy et al., 2014) instead of the regularized Coulomb law (Eq 1.1). We use the original initialization, but we locally prescribe friction coefficients in the Schoof law to match the basal friction from the regularized Coulomb law (Eq. 1.1).
Powerlaw

This run is similar to the one previously described, but with a new initialization where we tune for a constant C_p in the powerlaw (see Eq. S2, Schoof 2007), to test if the slightly different geometry and inversion impact the continuation. The powerlaw exponent *m* is set to 1/3. A new initial state is obtained.

$$\tau_b = C_p u_b^m \quad \text{(S2)}$$

Thermal forcing capped at the maximum found at the grounding line
We determine the thermal forcing of PIG and TG at the present-day grounding line, and the maximum value found in those basins (respectively 3.73 K and 4.10 K) is used as an upper limit for the thermal forcing in newly ungrounded cells, to test whether the interpolation of thermal forcing under present-day grounded ice is affecting the collapse.

Relaxed asthenosphere, relaxation time = 3000 yr
This run is done with an ELRA GIA model (Hagdorn, 2003), with a relaxation period of 3000 yr. This causes bedrock uplift rates of ~1 cm/yr. The original initialization is used, so we assume isostatic equilibrium at the end of our default initialized state.

Powerlaw, original initialization
This run is done with a classical powerlaw relation as in Eq. S2 between basal velocities and basal sliding (with an exponent *m* = 1/3). The original initialization is used, but the tuned parameter in the default sliding law is modified in such a way that at $t = 0$, the powerlaw and the default sliding law give the same basal friction.

SMB increase by 20%
The SMB over Antarctica is expected to increase with increasing temperatures in the future, so in this run we instantly increase the SMB by 20% at the start of the default continuation run. The original initialization is used.

Smaller flow factor (stiffer ice)
We apply a flow factor of 0.25 for floating ice and 0.5 for grounded ice. A new initial state is obtained.

Mass change rates only applied on the shelves
We apply the satellite-observed mass change rates only for floating ice, and not for grounded ice, during the transient spin-up. This results in higher values of the friction parameter C_c in regions where the ice is thinning.

8km-grid, floatation condition melt parameterization
We test the Floatation Condition Melt Parameterization (FCMP, see Leguy et al., 2021), where melt is applied only to cells whose centre is floating. This gives a step function in basal melt rates, compared to the smoothly changing rates in the PMP scheme. We run at 8-km resolution, with a new initial state.

Reduce basal melt rates after 50 years by 25%
We instantly decrease the calculated basal melt rates by 25% after running 50 years in the continuation run. The original initialization is used.

Floatation condition melt parameterization Similar to the *FCMP on 8-km* run, but run at the default 4-km resolution. A new initialization is used.
ELRA isostasy, relaxation time = 100 yr Similar to *Relaxed asthenosphere, relaxation time = 3000 yr,* but with a relaxation time of 100 years. This produces uplift rates exceeding 50 cm/yr. The original initialization is used.
Full ocean connection, p = 1 Similar to p = 0.5, but in this case with a full ocean connection (*p* = 1). A new initialization is used.
Low basal melt versus thermal forcing Similar to *High basal melt versus thermal forcing*, but with γ_0 = 10,000, close to the lowest value tested in (Jourdain et al., 2020). We use the original initialization and recalculate the ocean temperatures so the basal melt rates at *t* = 0 match those of the default run.
Decrease basal melt rates after 50 years by 50% Similar to *Decrease basal melt rates after 50 years by 25%,* but now we halve the basal melt rates. The original initialization is used.
No-melt parameterziation For this run we apply the No Melt Parameterization (Leguy et al., 2021), where no basal melting is applied in partly floating cells (i.e., cells that contain the grounding line). A new initialization is used.
8-km grid, no-melt parameterization 8-km Similar to *No-melt parameterziation,* but run at 8-km resolution. A new initialization is used.

References

Adusumilli, S., Fricker, H. A., Medley, B., Padman, L., and Siegfried, M. R.: Interannual variations in meltwater input to the Southern Ocean from Antarctic ice shelves, Nature geoscience, 13, 616-620, 2020.

Berdahl, M., Leguy, G., Lipscomb, W. H., Urban, N. M., and Hoffman, M. J.: Exploring ice sheet model sensitivity to ocean thermal forcing and basal sliding using the Community Ice Sheet Model (CISM), The Cryosphere, 17, 1513-1543, 2023.

Hagdorn, M. K.: Reconstruction of the past and forecast of the future European and British ice sheets and associated sea–level change, Edinburgh Research Archive, 2003.

Jourdain, N. C., Asay-Davis, X., Hattermann, T., Straneo, F., Seroussi, H., Little, C. M., and Nowicki, S.: A protocol for calculating basal melt rates in the ISMIP6 Antarctic ice sheet projections, The Cryosphere, 14, 3111-3134, 2020.

Leguy, G., Asay-Davis, X., and Lipscomb, W.: Parameterization of basal friction near grounding lines in a one-dimensional ice sheet model, The Cryosphere, 8, 1239-1259, 2014.

Leguy, G. R., Lipscomb, W. H., and Asay-Davis, X. S.: Marine ice sheet experiments with the Community Ice Sheet Model, The Cryosphere, 15, 3229-3253, 2021.
Morlighem, M., Rignot, E., Binder, T., Blankenship, D., Drews, R., Eagles, G., Eisen, O., Ferraccioli, F., Forsberg, R., and Fretwell, P.: Deep glacial troughs and stabilizing ridges unveiled beneath the margins of the Antarctic ice sheet, Nature Geoscience, 13, 132-137, 2020.
Rignot, E., Jacobs, S., Mouginot, J., and Scheuchl, B.: Ice-shelf melting around Antarctica, Science, 341, 266-270, 2013.
Rignot, E., Mouginot, J., Scheuchl, B., Van Den Broeke, M., Van Wessem, M. J., and Morlighem, M.: Four decades of Antarctic Ice Sheet mass balance from 1979–2017, Proceedings of the National Academy of Sciences, 116, 1095-1103, 2019.
Smith, B., Fricker, H. A., Gardner, A. S., Medley, B., Nilsson, J., Paolo, F. S., Holschuh, N., Adusumilli, S., Brunt, K., and Csatho, B.: Pervasive ice sheet mass loss reflects competing ocean and atmosphere processes, Science, 368, 1239-1242, 2020.